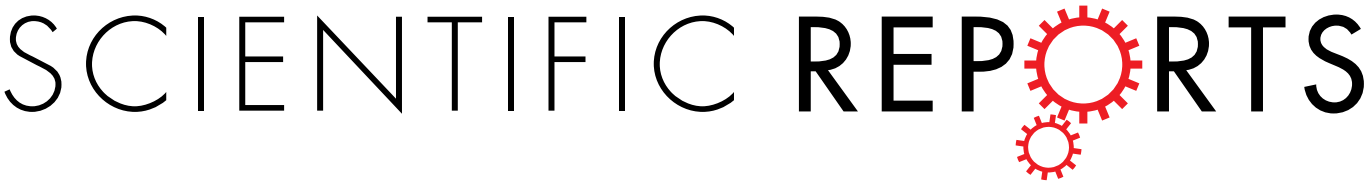

OPEN

Received: 30 December 2015
Accepted: 20 July 2016
Published: 17 August 2016

Assessment of agglomeration, co-sedimentation and trophic transfer of titanium dioxide nanoparticles in a laboratory-scale predator-prey model system

Govind Sharan Gupta[1,2], Ashutosh Kumar[1], Rishi Shanker[1] & Alok Dhawan[2]

Nano titanium dioxide ($nTiO_2$) is the most abundantly released engineered nanomaterial (ENM) in aquatic environments. Therefore, it is prudent to assess its fate and its effects on lower trophic-level organisms in the aquatic food chain. A predator-and-prey-based laboratory microcosm was established using *Paramecium caudatum* and *Escherichia coli* to evaluate the effects of $nTiO_2$. The surface interaction of $nTiO_2$ with *E. coli* significantly increased after the addition of *Paramecium* into the microcosm. This interaction favoured the hetero-agglomeration and co-sedimentation of $nTiO_2$. The extent of $nTiO_2$ agglomeration under experimental conditions was as follows: combined *E. coli* and *Paramecium* > *Paramecium* only > *E. coli* only > without *E. coli* or *Paramecium*. An increase in $nTiO_2$ internalisation in *Paramecium* cells was also observed in the presence or absence of *E. coli* cells. These interactions and $nTiO_2$ internalisation in *Paramecium* cells induced statistically significant ($p < 0.05$) effects on growth and the bacterial ingestion rate at 24 h. These findings provide new insights into the fate of $nTiO_2$ in the presence of bacterial-ciliate interactions in the aquatic environment.

Engineered nanomaterials (ENMs) are used in diverse applications, owing to their unique optical, chemical, mechanical, thermal, magnetic and catalytic properties[1]. Currently, more than 1800 nano-based consumer products derived from 45 different ENMs are manufactured globally[2]. ENMs can enter into the environment at various stages in their life cycle: production, manufacturing, transportation, consumer use and product disposal[3–5].

Nano titanium dioxide ($nTiO_2$) is one of the most abundant materials in products such as cosmetics, paints, food additives, pharmaceuticals, electronics, and textiles as well as in construction and wastewater treatment[6–8]. Moreover, the unique photocatalytic and UV-reflecting properties of $nTiO_2$ have enhanced the exponential growth of low-cost and safer consumer products[9–11]. Risk assessment studies have predicted $nTiO_2$ to be the most abundant ENM in the environment [21–10000 ng/L in surface water, 1–100 μg/L in waste water treatment plant (WWTP) effluent, 100–2000 mg/kg in WWTP sludge][12].

Aquatic environments act as a sinks for chemicals as well as emerging metal pollutants such as ENMs[13]. Aquatic bodies contain a dominant and ubiquitous community of bacteria (~10^6 cells/ ml) as well as the bacterial predators ciliated protozoans (10^2–10^4 cells/ml)[14,15]. ENMs affect the organisms within and across trophic levels in the aquatic food chain. Poor water solubility and long-term persistence of ENMs in aquatic systems[16,17] facilitate their bioaccumulation and biomagnification in aquatic organisms such as bacteria, ciliated protozoans, rotifers, algae, crustaceans, zebrafish, and mussels[18–24]. The accumulation of ENMs can also affect the growth, reproduction, ingestion and digestion behaviour of aquatic organisms[18,20,21]. Factors such as surface interactions (adsorption or hetero-agglomeration), internalisation, oxidative stress, membrane damage and mitochondrial perturbations have been reported to be responsible for the acute toxicity of ENMs in microorganisms, cell lines

[1]Division of Biological & Life Sciences, School of Arts & Sciences (Formerly, Institute of Life Sciences), Ahmedabad University, University Road, Navrangpura, Ahmedabad - 380009, Gujarat (India). [2]Nanotherapeutics & Nanomaterial Toxicology Group, CSIR-Indian Institute of Toxicology Research (CSIR-IITR), Vishvigyan Bhawan, 31-M.G. Marg, Lucknow - 226001, U.P. (India). Correspondence and requests for materials should be addressed to R.S. (email: rishi.shanker@ahduni.edu.in) or A.D. (email: alokdhawan@iitr.res.in)

Groups	1 h	24 h
$nTiO_2$-UZ	395 ± 8	299 ± 44
$nTiO_2$-MZ	411 ± 6	318 ± 41
$nTiO_2$-LZ	411 ± 9	402 ± 28
Ec + $nTiO_2$-UZ	699 ± 9**	425 ± 10
Ec + $nTiO_2$-MZ	521 ± 6**	530 ± 4*
Ec + $nTiO_2$-LZ	601 ± 6**	814 ± 15**
Pm + $nTiO_2$-UZ	742 ± 8**	734 ± 6**
Pm + $nTiO_2$-MZ	657 ± 11**	790 ± 19**
Pm + $nTiO_2$-LZ	781 ± 10**	1211 ± 47**
Ec + Pm + $nTiO_2$-UZ	1036 ± 27**	1138 ± 46**
Ec + Pm + $nTiO_2$-MZ	967 ± 6**	1400 ± 68**
Ec + Pm + $nTiO_2$-LZ	875 ± 17**	ND

Table 1. Hydrodynamic diameter (d-nm) of $nTiO_2$ in the microcosm, reflecting agglomeration. Pm, *Paramecium*, Ec, *E. coli*. ND, not detected. Values represented are the mean ± SE of three independent experiments. *$p < 0.05$ was considered significant compared with the control.

and eukaryotic organisms[25]. The surface interactions of ENMs with microbial cells, the first step in ENM toxicity, are predominantly governed by charge interactions between ENMs and microbes[26,27]. ENMs with positive surface charges have been found to have higher toxicities than ENMs with negative charges. This finding has been attributed to the negative charges of cell surfaces[28,29]. In the natural environment, bacterial cells are ubiquitously present and have a high ratio of surface area to their volume; thus, the cells interact with and absorb high levels of ENMs[15,30]. Additionally, the presence of exopolymeric substances (EPS) on the outer membranes of bacterial cells complements the adsorption of ENMs from the aquatic environment[15,31,32]. Ciliated protozoans such as *Tetrahymena* secrete mucus from their mucous membranes under stress conditions, and this surface coating affects the fate of ENMs in the medium[33].

To understand the actual behaviours and toxicities of ENMs in aquatic systems, it is necessary to study the surface interactions, such as adsorption and hetero-agglomeration, of ENMs with microorganisms. For instance, the physical properties of *E. coli* cells are affected by exposure to hematite nanoparticles (NPs)[34]. The adsorption of ENMs on the *E. coli* surface is dependent on size: large hematite NPs adsorb faster than smaller NPs do[32]. In another study conducted in *Paramecium multimicronucleatum*, $nTiO_2$ has been found not to cause toxicity, owing to weak surface interaction energy[35]. Furthermore, different pH and ionic strength conditions play roles in the hetero-agglomeration and co-sedimentation of discharged oxide nanoparticles with chlorella cells[36]. Studies examining the surface adsorption and hetero-agglomeration of ENMs with biotic factors have been limited to the single organism level.

No studies have examined the adsorption, hetero-agglomeration and co-sedimentation of ENMs in the presence of a predator-prey interaction model of a real-world environmental situation. Such an interaction model, involving two organisms in lower trophic levels of the food chain, can be represented by a bacterium and a ciliated protozoan. *E. coli* has been used extensively as a model bacterium in toxicity assessments of ENMs because it divides rapidly and is easily cultured[32,37]. *Paramecium caudatum,* a ubiquitous single-celled ciliated protozoan that feeds on bacteria, is a significant ecological link between microbes and multicellular organisms[33,35].

Therefore, in the present study, an experimental aquatic microcosm involving *Escherichia coli* as prey and *Paramecium caudatum* as a predator was established to understand the hetero-agglomeration and co-sedimentation of $nTiO_2$ in the presence of predator-prey interactions. The microcosm was also used to determine the bioavailability, trophic transfer and effect of $nTiO_2$ on the food chain.

Results and Discussion

Characteristics of $nTiO_2$. The commercial $nTiO_2$ used in the present study was heterogeneously distributed, with a particle distribution ranging from 100 nm to 400 nm, as determined by dynamic light scattering (DLS) analysis (SI-Fig. S2a). Transmission electron microscopy (TEM) indicated that most particles ranged from 10 to 70 nm, with an average size of 40 nm (SI-Fig. S2c). The zeta potential of $nTiO_2$ in Dryl's buffer was −31 mV (SI-Fig. S2b). The size of $nTiO_2$ determined by DLS was higher because of the formation of the hydrodynamic layer on its surface.

Rationale for selection of sampling time points. In all the experiments, the initial time point was 1 h to allow optimum adsorption of $nTiO_2$ on the surface of test organisms. The final time point was selected as 24 h, coinciding with the life cycle of *Paramecium*[38]. This duration was sufficient to allow recurrent ingestion and digestion of bacteria. It also ensured that nanoparticle agglomeration achieved a steady state[39].

Adsorption and hetero-agglomeration of $nTiO_2$ in the microcosm. The average hydrodynamic diameters of $nTiO_2$ agglomerates observed in different groups ($nTiO_2$, $nTiO_2$ + *E. coli,* $nTiO_2$ + *Paramecium* and $nTiO_2$ + *E. coli* + *Paramecium*) at 1 h and 24 h are presented in Table 1. A concomitant and significant ($p < 0.001$) increase in the size of $nTiO_2$ agglomerates was observed because of the presence of test organisms (*E. coli* and/or *Paramecium*) in the exposure medium. The agglomerate size of an individual $nTiO_2$ suspension at the initial time point (1 h) was uniform across all characterised zones (upper zone, UZ; middle zone, MZ and lower zone, LZ) of

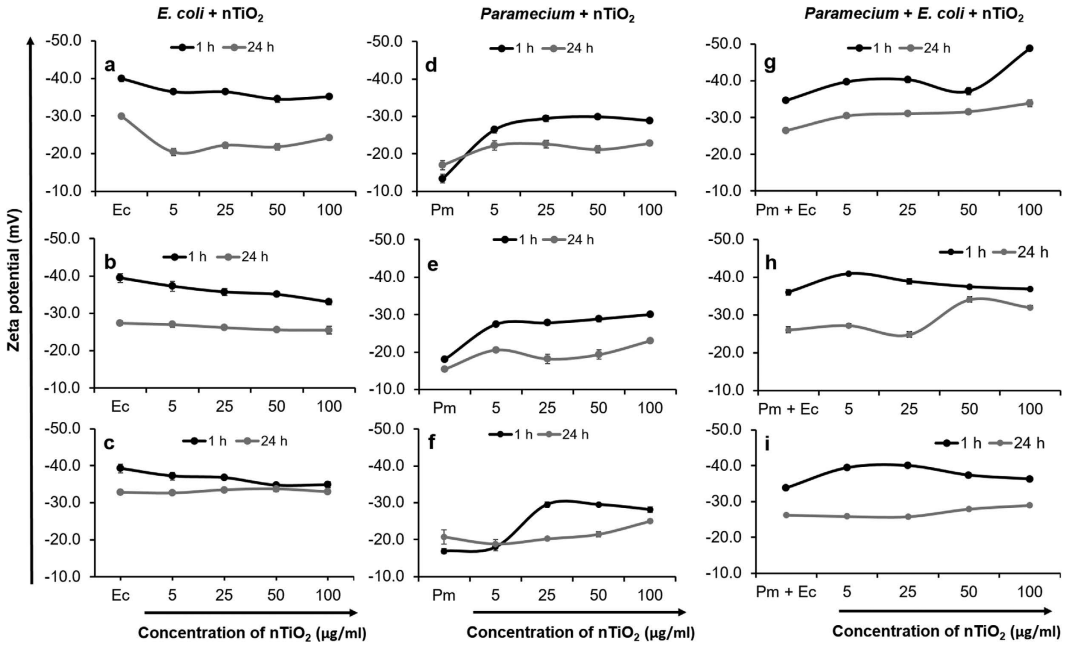

Figure 1. Zeta potential of $nTiO_2$ in different zones of the experimental tube at 1 h and 24 h. (**a–c**) $nTiO_2$ incubated with *E.* coli, (**d–f**) $nTiO_2$ incubated with *Paramecium*, (**g–i**) $nTiO_2$ incubated with *Paramecium* and *E. coli.* (**a,d,g**) = upper zone; (**b,e,h**) = middle zone and (**c,f,i**) = lower zone. Ec, *E. coli*, Pm, *Paramecium.* Values represented are the mean ± SE of three independent experiments.

the simple microcosm. However, a statistically significant ($p < 0.001$) increase in agglomerate size was observed after the addition of *E. coli* and *Paramecium* cells, individually or in combination.

At the final time point (24 h), the size of $nTiO_2$ agglomerates in the LZ of the microcosm increased significantly ($p < 0.001$), with sedimentation of larger agglomerates in all the groups ($nTiO_2$ + *E. coli*, $nTiO_2$ + *Paramecium* and $nTiO_2$ + *E. coli* + *Paramecium*) (Table 1). Sedimentation occurred because of the increased adsorption of $nTiO_2$ on the surface of the *E. coli* and the release of mucus exudates by *Paramecium* cells[33]. The agglomerate size observed in the lower zone was maximised at 24 h in the following order: $nTiO_2$ + *E. coli* + *Paramecium* > $nTiO_2$ + *Paramecium* > $nTiO_2$ + *E. coli*. The agglomerate size of $nTiO_2$ in the *Paramecium* co-incubation group was greater than that in the *E. coli* co-incubation group because of differences in binding interactions between $nTiO_2$ and organisms. The negatively charged surfaces of $nTiO_2$ (−32 mV) and *E. coli* (−39 mV) do not permit electrostatic interactions (SI-Figure S3 and Fig. 1). A weak electrostatic association may be possible between $nTiO_2$ (−32 mV) and *Paramecium* (−18 mV), given the extreme difference in the intensity of negative charges of both surfaces (Fig. 1d–f). Further, the combination of *Paramecium* with *E. coli* cells in the microcosm decreased the overall zeta-potential of *E. coli* in the absence of $nTiO_2$ but increased slightly after the addition of $nTiO_2$, possibly because of adsorption on the *E. coli* surface. This observation shows that poor electrostatic interactions between $nTiO_2$ and *E. coli* in the presence of *Paramecium* are possible (Fig. 1i). At 24 h, these interactions were negligible, owing to the equilibration of the overall charges between *E. coli* and $nTiO_2$ (Fig. 1c,i).

Previous studies have shown that *E. coli* cells produce exopolymeric substances that are involved in $nTiO_2$ adhesion[40–42]. Jucker *et al.*[43] and Host *et al.*[41] suggested that numerous bacterial exopolymers, such as lipopolysaccharides (LPS) and siderophores (in *Pseudomonas aeruginosa*), participate in the adsorption of $nTiO_2$ and other metals on the bacterial surface. Li and Logan[44] have observed that long-chain LPS in *E. coli* cells adheres more widely to $nTiO_2$ than short chain LPS. Hahn *et al.*[45] and Pernthaler[14] have also shown that the predation of planktonic bacteria by a ciliated protozoan in the aquatic environment induces the biosynthesis of exopolymeric substances in bacteria, which protect against predation by facilitating biofilm formation. In the present study, a similar mechanism may be responsible, thus facilitating the adsorption of $nTiO_2$ onto the *E. coli* surface in the presence of *Paramecium*.

The adsorption and hetero-agglomeration of $nTiO_2$ on the surface of organisms in the microcosm was further assessed through dark field (SI-Fig. S4) and scanning electron microscopy coupled with EDS (SEM-EDS) (Fig. 2). Dark field microscopy revealed the hetero-agglomeration of $nTiO_2$ after 1 h of incubation with *E. coli* and *Paramecium* cells (SI-Fig. S4). SEM-EDS observations further confirmed the hetero-agglomeration of $nTiO_2$ in the presence or absence of *E. coli* and *Paramecium* at 1 h (SI Figs S5 and S6) and 24 h (Fig. 2). The images showed the adsorption and agglomeration of $nTiO_2$ on the surface of *E. coli* and *Paramecium* cells within 1 h. Moreover, at 24 h, the size of the $nTiO_2$ agglomerates increased in co-incubated and individual suspensions (Table 1). The increased size of individual $nTiO_2$ agglomerates in suspension was attributable to homo-agglomeration in the presence of Na^+ and Ca^{++} ions in Dryl's buffer, which was used as an exposure medium throughout the experiments[36,46,47].

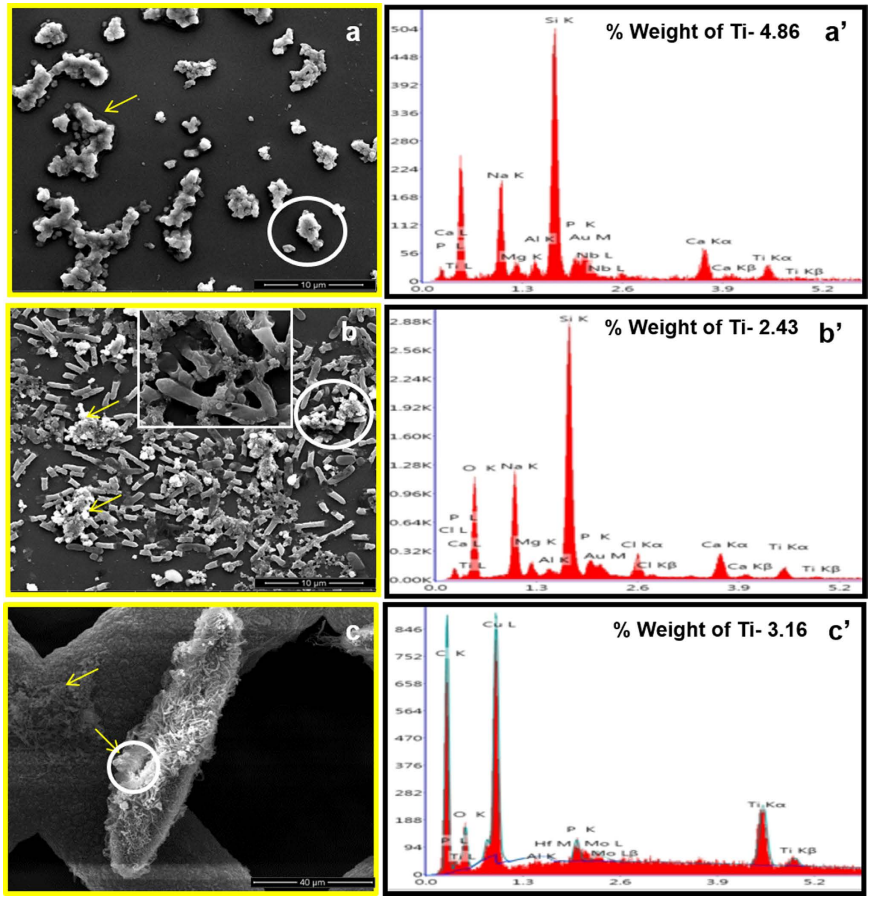

Figure 2. Adsorption and homo- and hetero-agglomeration of nTiO2 in an aquatic microcosm. SEM images with corresponding EDS spectra after 24 h of incubation with and without organisms. (**a**,a') $nTiO_2$ in Dryl's buffer, (**b**,b') $nTiO_2$ incubated with *E. coli* in Dryl's buffer, (**c**,c') $nTiO_2$ incubated with *E. coli* and *Paramecium* in Dryl's buffer. The white circle corresponds to the point where the EDS spectrum analysis was performed. The yellow arrow indicates $nTiO_2$ agglomerates. The inset image in (**b**) shows the surface interaction of $nTiO_2$ with *E. coli*.

Co-sedimentation of $nTiO_2$ in the microcosm. Figure 3 shows that the co-sedimentation of $nTiO_2$ occurred only with *E. coli* and not with *Paramecium* in the microcosm. This result may be attributed to the low motility of *E. coli* cells (25 μm/s) compared with the high motility of *Paramecium* cells in the water column (1.7 mm/s)[48,49]. The adsorption of $nTiO_2$ on the *E. coli* surface led to co-sedimentation because the presence of titanium was detected by EDS scanning of bacterial cells recovered from the LZ of the microcosm (Fig. 2).

$nTiO_2$ and *E. coli*. The most significant co-sedimentation of $nTiO_2$ with *E. coli* was obtained at 5 μg/ml $nTiO_2$, a concentration at which hetero-agglomeration is the favourable option, because of the availability of an optimum ratio between the number of nanoparticles and the surface area of *E. coli* cells (SI-Table S1). However, at higher concentrations (50 and 100 μg/ml) homo-agglomeration was favoured, owing to dominant nanoparticles-nanoparticle interactions that reduced the co-sedimentation of NPs with *E. coli* cells (SI-Fig. S9b). These observations are consistent with results from previous studies examining the homo- and hetero-agglomeration of ENMs[39,40,47,50]. Furthermore, the analysis of additive sedimentation of *E. coli* and $nTiO_2$ permitted the calculation of nanoparticle-cell interactions, thus supporting our findings regarding hetero-agglomeration (Fig. 3d)[36]. The maximum interaction of *E. coli* with $nTiO_2$ was observed at the lowest concentration of $nTiO_2$ (5 μg/ml), as evident in the discrepancy (ΔOD) between $nTiO_2$-bacteria co-sedimentation and additive settling in the LZ (Table 2). $\Delta OD > 0$ represents the occurrence of NP−cell hetero-agglomeration and co-sedimentation, whereas zero or negative ΔOD values indicate no or very weak agglomeration between NPs and cells[36].

$nTiO_2$ and *Paramecium*. Co-sedimentation of $nTiO_2$ was not observed with *Paramecium* in the absence of *E. coli* because the ΔOD value was highly negative (> -0.85; Table 2) for all concentrations of $nTiO_2$ (Fig. 3b). Slight sedimentation of $nTiO_2$ in LZ was observed at higher concentrations (50 and 100 μg/ml; Fig. 3b). This observation may be attributable to the continuous release of larger $nTiO_2$-loaded vesicles from the cytoproct region of the *Paramecium*, which is a normal physiological process to egest un-digested material (SI-Fig. S10c,d). These vesicles are covered with the mucous membrane, which may further influence agglomeration in exposure medium[33,51].

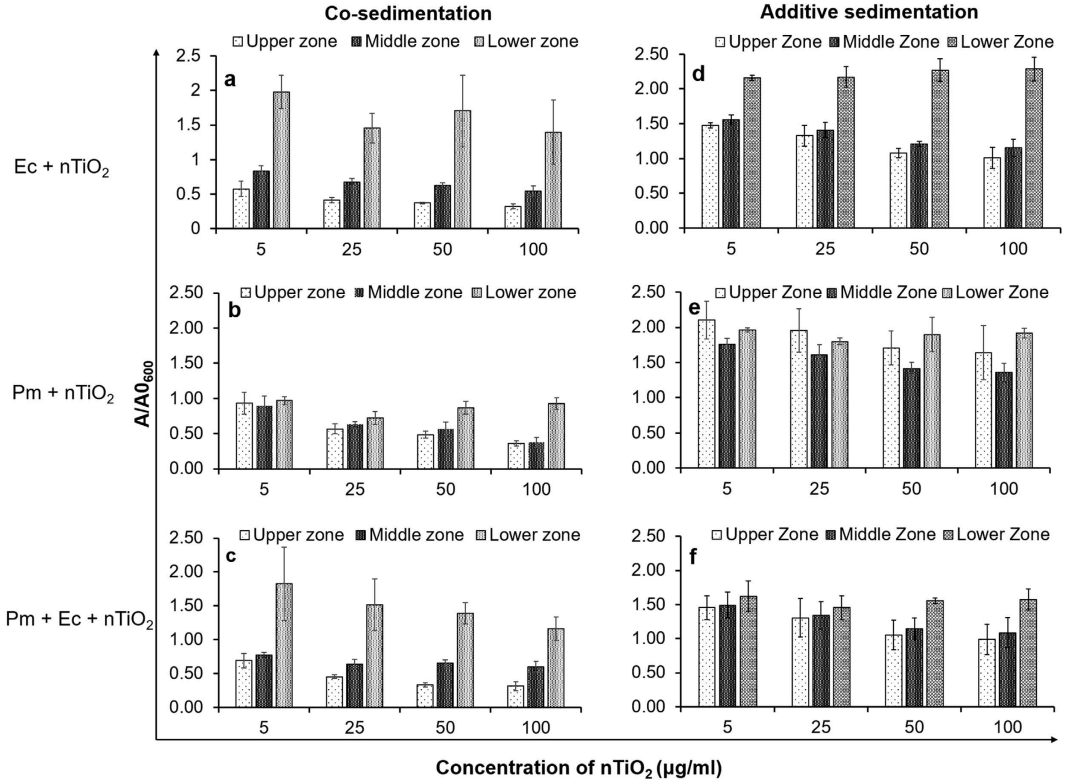

Figure 3. Co-sedimentation (a–c) and additive-sedimentation (d–f) plots of $nTiO_2$ in the presence of *E. coli* and *Paramecium* in an aquatic microcosm. The ratio of initial to final absorbance at 600 nm in the upper, middle and lower zones of the microcosm depicting the effects of *E. coli* and *Paramecium* individually and in combination on the sedimentation of $nTiO_2$. Ec, *E. coli*, Pm, *Paramecium*. Values represented are the mean ± SE of three independent experiments.

Concentration of $nTiO_2$ (µg/ml)	*E. coli* + $nTiO_2$			*Paramecium* + $nTiO_2$			*Paramecium* + *E. coli* + $nTiO_2$		
	Upper Zone	Middle Zone	Lower Zone	Upper Zone	Middle Zone	Lower Zone	Upper Zone	Middle Zone	Lower Zone
5	−0.90	−0.73	−0.18	−1.17	−0.87	−1.00	−0.76	−0.72	0.20
25	−0.91	−0.74	−0.71	−1.39	−0.98	−1.08	−0.85	−0.70	0.06
50	−0.71	−0.59	−0.56	−1.22	−0.85	−1.04	−0.72	−0.49	−0.16
100	−0.69	−0.61	−0.89	−1.27	−0.98	−0.99	−0.67	−0.49	−0.41

Table 2. Differences (ΔOD) in the A/A_0 values of co- and additive sedimentation of $nTiO_2$ in an aquatic microcosm. Values represented are the mean ± SE of three independent experiments. A/A_0 = Final absorbance/Initial absorbance.

$nTiO_2$ in combination with *Paramecium* and *E. coli*. A significant increase in the co-sedimentation of $nTiO_2$ with *E. coli* cells was observed in the presence of *Paramecium*, as evidenced by the high positive ΔOD (0.20) value at the lowest concentration of $nTiO_2$ (5 µg/ml), although the ΔOD value was close to zero (0.06) at 25 µg/ml (Table 2; Fig. 3c). This result indicated that the interaction of $nTiO_2$ with *E. coli* was stronger in the presence of *Paramecium* at lower concentrations. The enhanced interaction and hetero-agglomeration of $nTiO_2$ on the surface of *E. coli* in the presence of a predator species (*Paramecium*) indicated that the biotic interactions of $nTiO_2$ in aquatic systems influence the fate as well as toxicity of this NP in bacteria and other organisms. These observations are supported by an earlier report examining the effects of surface interactions between nanoparticles and bacteria on toxicity[27]. In addition, co-sedimentation of $nTiO_2$ may adversely affect sediment dwelling organisms[52].

The interaction of $nTiO_2$ with *Paramecium* in the presence of *E. coli* was also observed by using dark field and scanning electron microscopy. The dark field microscopy demonstrated that $nTiO_2$ was taken up by *Paramecium* in the form of vesicles (SI-Fig. S4c,d), which were later released from the cytoproct in the form of aggregates. Further, SEM-EDS revealed the presence of $nTiO_2$ in the oral groove regions of *Paramecium* cells, thus indicating its internalisation via phagocytosis (Fig. 2c,c' & SI-Fig. S8c). Phagocytosis is a well-defined mechanism for NP uptake in ciliates such as *Tetrahymena*[33].

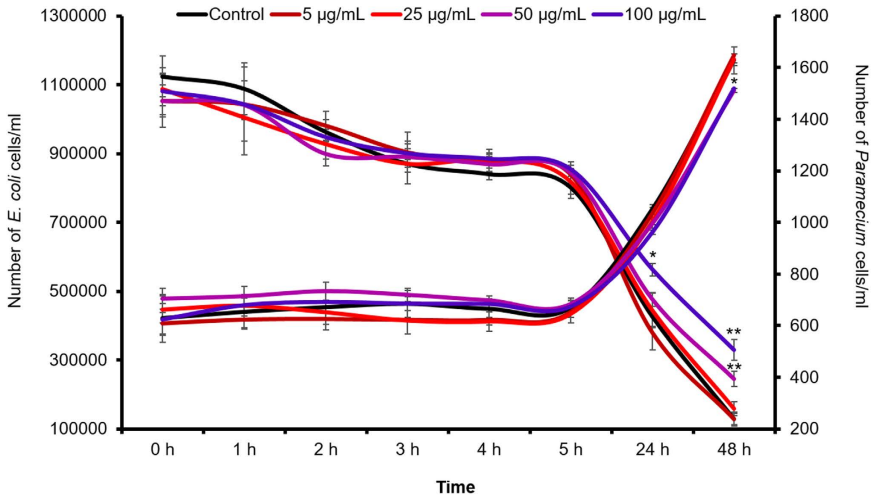

Figure 4. Growth and bacterial ingestion rate of *Paramecium* cells after exposure to $nTiO_2$ at different concentrations. Values represented are the mean ± SE of the three independent experiments. *$p < 0.05$ was considered significant compared with control.

The behaviour of the test organisms in the presence or absence of $nTiO_2$ in the microcosm was also determined. The observations revealed that *Paramecium* cells remained alive throughout the experiment as there were no signs of mortality, such as membrane leakage or loss of motility, at the tested time points. Furthermore, measurements revealed compromised bacterial ingestion and growth of *Paramecium* at 24 h after exposure to a higher dose of $nTiO_2$ (100 µg/ml; Fig. 4). The *Paramecium* ingestion rate was ~1600 bacterial cells/ciliate/h. The morphological observation of *E. coli* cells by SEM revealed the shrinking size of *E. coli* cells recovered at 24 h from the LZ of the microcosm (SI-Figs S7a and S8a,b). This effect was also observed in the DLS analysis, which showed a decrease in the size of *E. coli* cells (SI- Table S2).

The shrinking and co-sedimentation of *E. coli* cells in the presence of $nTiO_2$ may be attributable to the adsorption of NPs on the *E. coli* surface, thus affecting their physico-mechanical properties and possibly play a critical role in maintaining the cellular morphology and motility of bacterial cells. In an earlier study, Zhang *et al.*[34] have shown that the adsorption of hematite nanoparticles on the *E. coli* surface exerts multiple effects on physiological and mechanical properties, such as the loss of adhesiveness, elasticity, hardness, electrical potential and deformities in appendages such as flagella. These effects have the potential to inflict numerous consequences on bacterial cells, such as the loss of cellular motility, adhesion to surfaces and stability. The compromised motility and stability of bacterial cells due to the adsorption of nanoparticles may underlie the co-sedimentation of *E. coli* cells with $nTiO_2$. Protistan grazing on bacterial cells in the environment has been shown to affect the morphology, physiological behaviour and activity of bacterial cells[53]. In general, bacterivorous protists preferentially feed on medium-size bacterial cells rather than smaller or larger bacteria. In this context, del George *et al.*[54] have suggested that bacterial cells become inactive and thus adapt to powerful grazing pressure generated by the efficient grazing of bacteria by protists. Further, Gasol *et al.*[55] have shown that inactive bacterial cells are smaller than active cells. Therefore, the presence of *Paramecium* in the microcosm facilitates the shrinking and co-sedimentation of *E. coli* cells with $nTiO_2$.

The natural assemblage contains diverse communities that include motile, less-motile and sessile organisms in similar or diverse habitats. Therefore, under natural conditions, sessile organisms may also promote the co-sedimentation of NPs after interactions. To test this hypothesis, the adsorption of $nTiO_2$ on sessile embryos (4 h post-fertilisation) of an established zebrafish ecotoxicity model was evaluated. Preliminary observations using optical and scanning electron microscopy revealed the extensive binding of $nTiO_2$ on the chorion, which protects early stage embryos (SI-Figs S11 and 12). The presence of titanium on the chorion surface was further confirmed by EDS analysis (SI-Fig. S12). Therefore, it can be reasoned that interactions and co-sedimentation in water columns are mediated by members of the natural assemblage, including the highly motile *Paramecium* and less-motile organisms such as *E. coli* or sessile zebrafish embryos.

Previous studies have demonstrated that the fate and toxicity of ENMs may change because of the presence of natural colloids and organic matter in the environment[56]. The present study elucidated the role of predator-prey interactions in the hetero-agglomeration and co-sedimentation of ENMs in an aquatic environment. The findings also suggest that the adsorption and internalisation of $nTiO_2$ on highly motile *Paramecium* cells may further increase bioavailability to higher trophic level organisms in the food chain.

Real-time monitoring of $nTiO_2$ intracellular interactions in *Paramecium*

Internalisation of $nTiO_2$ in Paramecium in the absence of *E. coli*. Flow cytometry is a well-established technique to measure the cellular density of cells and microbes. The side scattering intensity (SSC-intensity) parameter correlates with changes in cellular granularity due to the uptake of nanoparticles[57,58]. The real-time monitoring of $nTiO_2$-exposed *Paramecium* cells in a flow cytometer revealed a dose-dependent and statistically significant ($p < 0.05$) increase in SSC-intensity, thus demonstrating the cellular internalisation of $nTiO_2$ (Fig. 5.1a). The

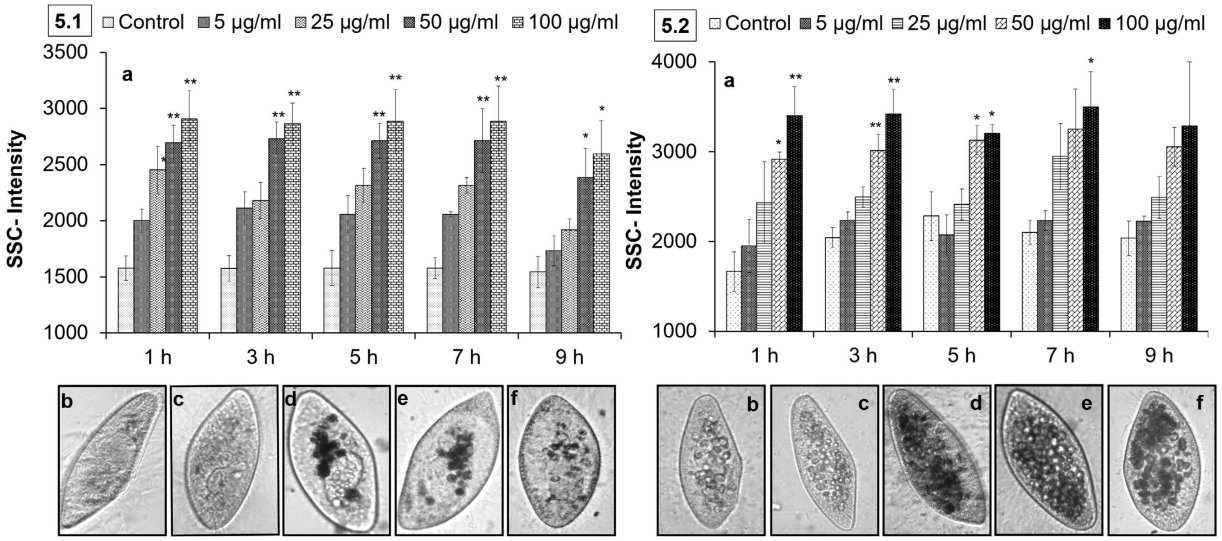

Figure 5. Real-time monitoring of $nTiO_2$ intracellular interactions in *Paramecium*. (5.1) Direct exposure of *Paramecium* cells to $nTiO_2$ up to 9 h. (a) A concentration-dependent and statistically significant ($p < 0.05$) increase in the internalisation of $nTiO_2$ in cells determined by flow cytometry. (b–f) Internalisation of $nTiO_2$ confirmed by bright field microscopy: (b,c) controls at 1 and 9 h, (d–f) 50 µg/ml-treated cells captured at 1, 7 and 9 h. **(5.2)** Exposure of *Paramecium* cells to $nTiO_2$ through Dryl's buffer and *E. coli* up to 9 h. (a) A concentration dependent and significant ($p < 0.05$) increase in the internalisation and retention of $nTiO_2$ in cells determined by flow cytometry. (b–f) Internalisation of $nTiO_2$ confirmed by bright field microscopy: (b,c) controls at 1 and 9 h, (d–f) 50 µg/ml-treated cells captured at 1, 7 and 9 h. (All bright field microscopy images were captured at 200x magnification). Values represented are the mean ± SE of three independent experiments. *$p < 0.05$ was considered significant compared to the control.

SSC-intensity was ~0.8-fold higher at an exposure concentration of 100 µg/ml compared with control conditions at 1 h. Further, the intensity of SSC remained constant up to 5 h, possibly because of the saturated uptake of $nTiO_2$ within 1 h, as represented by the dark vesicles packed into the cytoplasm of $nTiO_2$-treated *Paramecium* (Fig. 5.1b–e). At 7 h, a decrease in intracellular levels of $nTiO_2$ was observed, evidenced by a reduction in the number of dark cytoplasmic vesicles and a consistent decrease in the SSC-intensity of *Paramecium* cells (Fig. 5.1a,f). The reduction in the intracellular levels of $nTiO_2$ in *Paramecium* cells was attributable to the egestion of NPs loaded with undigested food vacuoles from the cytoproct and was confirmed by images captured through dark (SI-Figure S4d) and bright field microscopy (SI-Fig. S10c). The uptake rate of $nTiO_2$ was also decreased after 7 h because of agglomeration and co-sedimentation, as evidenced by DLS measurements (Table 1) and observations under bright field microscopy (SI-Fig. S10d).

Internalisation of $nTiO_2$ in *Paramecium* through exposure medium and *E. coli*. Figure 5.2 shows a concentration-dependent (5, 10, 50 and 100 µg/ml), statistically significant ($p < 0.05$) increase in the SSC-intensity of *Paramecium* cells exposed to $nTiO_2$ in the presence of *E. coli* cells. The *Paramecium* cellular density increased because of the internalisation of nanoparticles. The SSC-intensity of the *Paramecium* cells exposed to 100 µg/ml $nTiO_2$ was 1.04-fold higher than that of the control. This result demonstrated that the density of nanoparticles within *Paramecium* cells was slightly higher in the presence of *E. coli* than direct exposure (*Paramecium* + $nTiO_2$). Thus, additional exposure through feeding was involved in the uptake of nanoparticles into *Paramecium* cells. The internalisation of $nTiO_2$ was maximal at 1 h and remained constant up to 9 h in contrast to 7 h after direct exposure in the absence of *E. coli* (Fig. 5.2a and 5.1a). Under co-exposure (*Paramecium* + *E. coli* + $nTiO_2$) conditions, the retention of $nTiO_2$ in *Paramecium* cells was extended because of the presence of $nTiO_2$ and *E. coli* cells (Fig. 5.2b–f).

In addition, $nTiO_2$ bioavailability through *E. coli* was observed after the exposure of *Paramecium* cells to $nTiO_2$-pre-exposed *E. coli*. Figure 6 shows an increase in the SSC-intensity of *Paramecium* within 1 h of exposure to $nTiO_2$-pre-exposed *E. coli* and was significantly ($p < 0.05$) constant for more than 9 h. An increase in the cellular density of *Paramecium* cells was attributable to the transfer of $nTiO_2$ from *E. coli* cells. *E. coli* cells adsorb a mass of $nTiO_2$ within 1 h of exposure that is further transferred to their predator protozoan via phagocytosis[33]. Further, the digestion of ingested bacteria in *Paramecium* cells is complete within 1 h, and thus $nTiO_2$ is released from *E. coli*[59]. There is increased biocompatibility between nanoparticles and *Paramecium* cells, owing to the presence of bacterial components on the surface that prevent immediate release from the cytoproct of *Paramecium* cells. Here, the SSC-intensity of *Paramecium* cells was normalised to control levels at 24 h compared to 7 and 9 h under direct and co-exposure conditions. The cytoplasmic vacuoles of treated *Paramecium* cells also returned to control levels at 24 (Fig. 5b–f). Overall, the presence of a prey species (*E. coli*) plays significant role in the bioavailability and persistence of $nTiO_2$ in a predator (*Paramecium*). These observations also provide evidence, supporting the trophic transfer of $nTiO_2$ during prey-predator interactions.

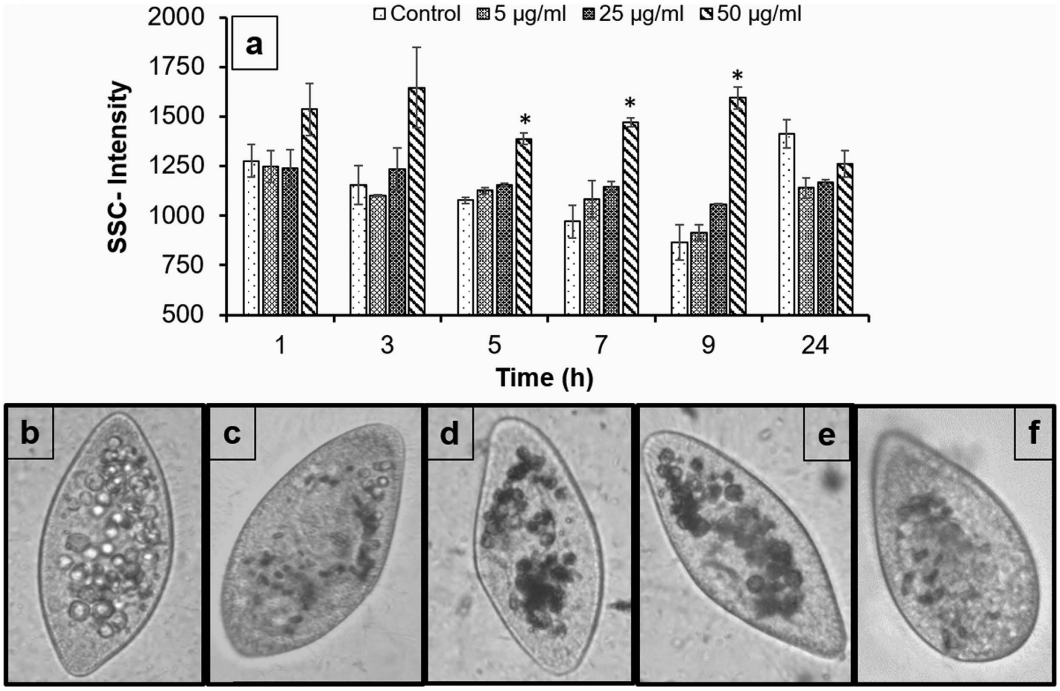

Figure 6. Trophic transfer of $nTiO_2$ in *Paramecium* relative to *E. coli*. (**a**) A statistically significant ($p < 0.05$) increase in the cellular granularity of *Paramecium* cells fed with $nTiO_2$-contaminated *E. coli* as determined by flow cytometry. (**b–f**) Trophic transfer of $nTiO_2$ further confirmed by bright field microscopy: (**b,c**) controls at 1 and 24 h, (**d–f**) 50 µg/ml-treated cells captured at 1, 7 and 24 h. (All bright field microscopy images were captured at 200x magnification). Values represented are the mean ± SE of the three independent experiments. *$p < 0.05$ was considered significant compared with control.

Transmission electron microscopy further confirmed the presence of $nTiO_2$, *E. coli* and $nTiO_2$-containing *E. coli* in the food vacuoles of *Paramecium* (Fig. 7a–f). TEM images clearly revealed the presence of $nTiO_2$ inside and outside the *E. coli* cells as well as those lodged in the food vacuoles of *Paramecium* cells, thus indicating that NPs were internalised into the cells either directly from Dryl's buffer or through *E. coli* (Fig. 7e,f). The role of *E. coli* as a vehicle for the transfer of $nTiO_2$ to *Paramecium* cells establishes the trophic transfer of $nTiO_2$ from the lower to the upper trophic levels in the microbial food chain. The trophic transfer of $nTiO_2$ was further supported by the presence of packaged bacteria and $nTiO_2$ in the egested *Paramecium* food vacuoles (SI-Fig. S10a).

Conclusion

Bacterial abundance and their high surface-area-to-volume ratio increases the probability of interactions with ENMs in the environment. The magnitude of interaction between ENMs and the bacterial surface can significantly alter the environmental fate and consequent toxicity of ENMs. Bacteria are the simplest organisms in the lower trophic levels linked to ciliated protozoans in the upper trophic levels of the food chain. The present study demonstrates that the presence of a predator, *Paramecium*, significantly influences the surface interactions between $nTiO_2$ and its prey, *E. coli*. The increased surface interactions between $nTiO_2$ and *E. coli* further enhanced the hetero-agglomeration and co-sedimentation of $nTiO_2$ in the modelled predator-prey-based microcosm. Although co-sedimentation reduces the bioavailability of $nTiO_2$ to organisms present in surface water columns, sediment-dwelling organisms may be at a higher risk of exposure to $nTiO_2$. The strong adsorption and internalisation of $nTiO_2$ in *Paramecium* cells increases the bioavailability of $nTiO_2$ via *Paramecium* to organisms such as rotifers and fish larvae, which are present at higher trophic levels in the food chain. The present study addresses a one-consumer (protozoan), one-resource (bacterium) system to assess the fate of $nTiO_2$. However, in a real-world situation, the effects of predation and interactions with prey species may be much greater than those observed in composite natural communities.

Methods

Chemicals and biological materials. Titanium dioxide nanopowder (anatase; 99.7%; CAS No. 1317-70-0) was purchased from Sigma Aldrich (St. Louis, USA). The *E. coli* K12 substrain DH10B was purchased from the Microbial Type Culture Collection Centre (MTCC, Chandigarh, India). *Paramecium caudatum* and protozoan pellets were purchased from Carolina Biological Supply Co. (Burlington, USA). Details regarding the use of *E. coli* and *Paramecium* as model organisms are provided in the supplementary information (SI-method section 1). All other chemicals were of analytical reagent grade and purchased from HiMedia Pvt. Ltd. (Mumbai, India).

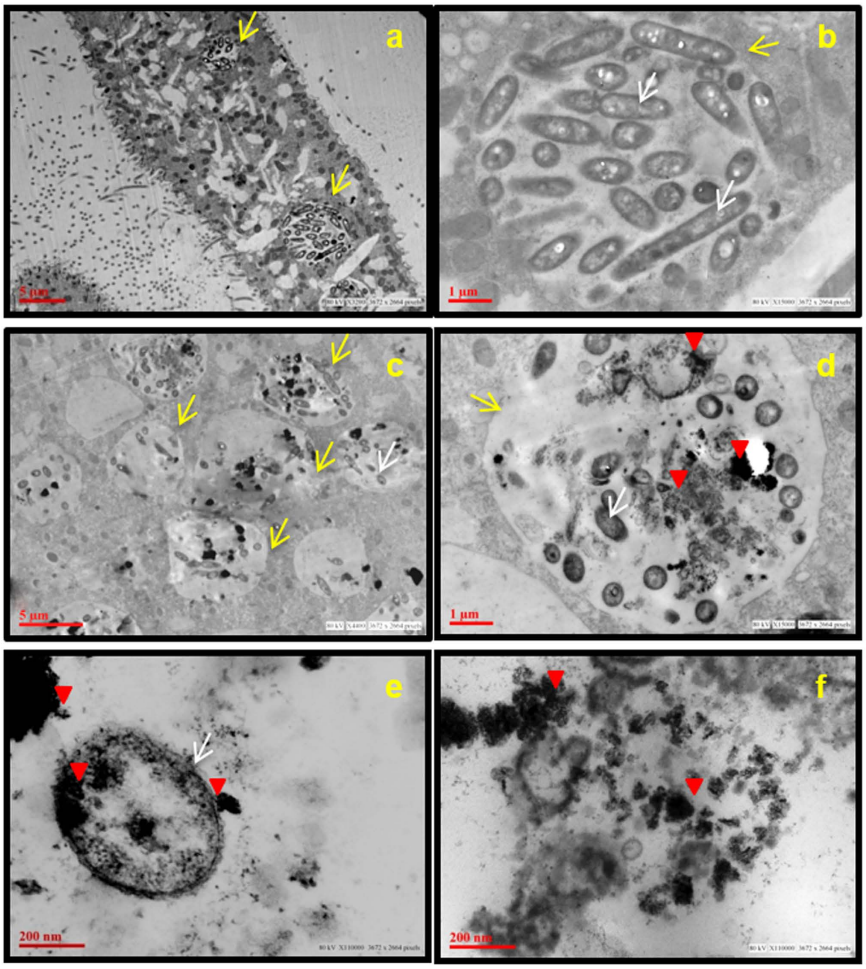

Figure 7. The interaction of *Paramecium* with *E. coli* and $nTiO_2$ after 1 h of incubation. Transmission electron microscopy images, **(a,b)** control, and **(c–f)** treated cells (25 µg/ml) showing the presence of *E. coli* and $nTiO_2$ in food vacuoles (**c,d**). $nTiO_2$ is present inside (**e**) and outside *E. coli* cells (**f**). Red arrowhead represents $nTiO_2$, yellow arrow represents food vacuoles and white arrow represents bacteria.

***E. coli* and *Paramecium* culture.** *E. coli* cells were cultured in Luria Bertani (LB) broth (HiMedia Pvt. Ltd., Mumbai, India) at 37 °C in an environmental shaker incubator. *Paramecium caudatum* was cultured in a protozoan pellet medium at 22 °C in a BOD incubator (Model LBI-500M, Daihan Labtech, India). A detailed protocol for medium preparation and *E. coli* and *Paramecium* culture is given in the supplementary information (SI-method section 2).

Nanoparticle preparation and characterisation. A stock suspension of 200 µg/ml $nTiO_2$ was prepared by adding 8 mg of $nTiO_2$ powder (anatase) to 40 ml of filtered Dryl's buffer (0.22-µm membrane filter). The suspension was then sonicated for 10 min using a probe sonicator (Sonics Vibra Cell, Sonics & Material Inc., New Town, USA) at 30% amplitude and 30 watts at a pulse rate of 50 sec on and 10 sec off. Before use, the suspension was maintained in a BOD incubator for 10 min to optimise the temperature to 22 °C. Subsequently, it was diluted to four different working concentrations of 5, 25, 50 and 100 µg/ml. A detailed description of the selection of concentrations is given in the supplementary information (SI-results section 2.0).

Hydrodynamic size and zeta potential were measured by dynamic light scattering (DLS) and phase analysis light scattering (PALS) using a Zeta-sizer Nano-ZS equipped with a 4.0-mW, 633-nm laser (Model ZEN3600; Malvern Instruments, UK). The distribution of different sizes of $nTiO_2$ was also observed by transmission electron microscopy (TEM). The samples for TEM analysis were prepared as described by Shukla *et al.*[58]. Briefly, a drop of $nTiO_2$ suspension (25 µg/ml) was placed on a formvar-coated copper grid. The film on the TEM grid was allowed to dry in the dark at room temperature. Images were captured using a Tecnai™ G2 Spirit electron microscopy (FEI, The Netherlands) at an accelerating voltage of 80 kV.

Microcosm setup. A simple aquatic microcosm was designed in a 50-ml polystyrene tube to assess the effects of biotic factors on the fate and stability of $nTiO_2$. The experiments were conducted in Dryl's buffer in seven different groups at 22 °C in a BOD incubator (LabTeK, India). Each group contained a 40-ml suspension of $nTiO_2$ or Dryl's buffer as well as predator-prey organisms and was marked into three zones, an upper zone

(UZ), a middle zone (MZ) and a lower zone (LZ), as shown in the supplementary information (SI Fig. S1). One millilitre of sample was withdrawn carefully from each zone at 1 h and 24 h for analysis. Dryl's buffer was used because of its unique chemical composition [sodium citrate (2 mM), NaH_2PO_4•H_2O (1 mM), Na_2HPO_4 (1 mM), $CaCl_2$ (1.5 mM), pH 7–7.2], which helps organisms to survive without stress for long durations, and the presence of citrate ions maintains the environmental relevance of the study because citrate is present in abundance in the natural environment[39]. Detailed information on the microcosm setup is given in the supplementary information (SI-method section 3).

Group 1: $nTiO_2$
Group 2: *E. coli*
Group 3: *E. coli* + $nTiO_2$
Group 4: *Paramecium*
Group 5: *Paramecium* + $nTiO_2$
Group 6: *Paramecium* + *E. coli*
Group 7: *Paramecium* + *E. coli* + $nTiO_2$

Measurement and analysis of $nTiO_2$ agglomeration and adsorption onto organisms in the microcosm. The agglomeration of $nTiO_2$ in the microcosm was measured by dynamic light scattering, which was further validated by dark field microscopy and scanning electron microscopy (SEM). The SEM was equipped with an energy-dispersive X-ray spectroscope (EDS), which complemented the qualitative images with compositional analysis of the adsorption of $nTiO_2$.

Sample preparation and analysis of hydrodynamic diameter and electro-kinetic measurements. Nanoparticle suspensions at different working concentrations were incubated with organism/s according to the experimental setup described for groups 2, 5 and 7 to measure the hetero-agglomeration.

Samples for analysis were withdrawn from each group at the initial (1 h) and final time points (24 h) from three different zones (upper, middle and lower) in the microcosm. The samples were analysed immediately using a Zeta-sizer Nano-ZS equipped with a 4.0-mW, 633-nm laser (Model ZEN3600, Malvern instruments Ltd., Malvern, UK). The zeta-sizer was equipped with a He–Ne laser (wavelength 633 nm) with a scattering angle of 173° and a constant temperature of 25 ± 1 °C. Water was selected as the experimental medium, with a refractive index of 1.330, and the refractive index of $nTiO_2$ was 0.200. A minimum of ten runs per analysis was carried out in automatic mode, and the data were analysed using the Zetasizer Software version 7.01 (Malvern, UK).

Measurement of hydrodynamic diameter. Measurements of the z-average intensity-based hydrodynamic size and size distribution were carried out with the DLS on the basis of the Stokes-Einstein equation. The modality of $nTiO_2$ size measurement by DLS was also verified by running *E. coli* and *Paramecium*. The multi-modal peaks of the individual organisms before and after incubation with $nTiO_2$ did not interfere with the measurement of $nTiO_2$ agglomeration, as shown in the supplementary information (SI Fig. S13). Given that the detection limit of the DLS equipment was ~8 μm, *Paramecium* cells could not be detected because of their large size (length ~110 μm and width ~40 μm) (SI-Fig. S7b and Table S2). *E. coli* was represented by a small peak in the size range of 2–6 μm by DLS (SI-Fig. S13 and Table S2) and 3–5 μm in length and ~0.7 μm in width by SEM (SI-Fig. S7a). The addition of *E. coli* did not interfere with the measurement of $nTiO_2$, owing to differences in the refractive index of *E. coli*. In an earlier study examining hematite nanoparticles, similar measurements were performed by DLS for bacterial cells[34]. The data are presented as the mean ± standard error of three independent experiments.

Zeta potential measurements. Zeta potential measures the total surface charge on particles and is independent of nanoparticle size and shape.[42]Zeta potential changes if the chemistry of the exposure medium is altered. The zeta potential of $nTiO_2$ and *E. coli* was measured in Dryl's buffer. Briefly, 1 ml of sample was injected into a capillary zeta cell (Folded Capillary Cell, DTS 1060, Malvern, UK). During injection of the sample, caution was taken so that bubbles did not form in the capillary cells and interfere with the analysis. Data were generated in the form of electrophoretic mobility, which was further converted to zeta potential by application of the Smoluchowki equation[41].

Microscopic observation and sample preparation. Samples from different zones of the microcosm were taken at 1 h and 24 h and analysed for homo- and hetero-agglomerates using dark field microscopy as well as scanning electron microscopy linked with energy dispersive X-ray spectroscopy (SEM-EDS).

Detailed protocols for sample preparation for dark field microscopy and SEM are given in the supplementary information (SI method section 4.1 and 4.2).

Measurement and analysis of $nTiO_2$ co-sedimentation and hetero-agglomeration in the microcosm. The experiments were carried out in the established microcosm as described above, with seven distinct groups. Four different concentrations of $nTiO_2$ (5, 25, 50 and 100 μg/ml) were used to determine the effects of $nTiO_2$ dilution on co-sedimentation.

Samples from each group and all zones were withdrawn at the initial (1 h) and final time points (24 h), immediately transferred to a quartz cuvette with a 1-cm path-length, and the absorbance was recorded at 600 nm using a UV-Vis spectrophotometer (Synergy HT, BioTek, Winooski, USA).

Co-sedimentation. Individual sedimentation and co-sedimentation patterns of $nTiO_2$ were measured and plotted using the method described by Ma *et al.*[36] with minor modifications. Briefly, the ordinate was calculated as the ratio of absorbance at a given time point (A) to the initial absorbance (A_0), and the graph was plotted against the concentrations of the $nTiO_2$. Independently, an additive sedimentation curve was also plotted as the sum of the individual absorbance of two different groups.

Hetero-agglomeration. The hetero-agglomeration of $nTiO_2$ with *E. coli* in the microcosm was measured as described by Ma *et al.* in algae[36]. The difference (ODmix-ODsum) between co-sedimentation [co-(ODmix)] and additive sedimentation [additive-(ODsum)] was calculated to determine the intensities of NP-cell interactions.

Measurement of bacterial ingestion rate of *Paramecium* cells. The assay was performed by counting the numbers of bacterial and *Paramecium* cells/ml in the control (*Paramecium* + *E. coli*) and treated (*Paramecium* + *E. coli* + $nTiO_2$ at 5, 25, 50 and 100 μg/ml) groups at 0, 1, 2, 3, 4, 5, 24 and 48 h after incubation. At each time point, 2 ml of culture was withdrawn from each group and divided into two separate 1-ml Eppendorf tubes. Separate tubes were used to count *Paramecium* and bacterial cells. The detailed protocol for bacterial and *Paramecium* cell counting is given in the supplementary information (SI-Method 2.1). To show the growth of *Paramecium* cells and the reduction in *E. coli* cells over time, a graph was plotted with the number of *E. coli* and *Paramecium* cells/ml on a double y-axis and time (h) on the x-axis.

The ingestion rate of *Paramecium* was determined by applying the formula suggested by Ali & Saleh[60].

$$Ingestion\ rate\ (bacteria/ciliate/h)\ I.R. = Nt - N0/t\,(h) \times 1/Np$$

N0 = number of prey (bacteria) at 0 h; Nt = number of prey (bacteria) at time (t);
Np = number of predators (bacterivorous ciliate).

Uptake of $nTiO_2$ in *Paramecium* cells via direct exposure and co-exposure. An experiment was designed to determine the intracellular fate of $nTiO_2$ in *Paramecium* cells under three different exposure conditions: (1) direct exposure of *Paramecium* cells to $nTiO_2$ in Dryl's buffer, (2) co-exposure of *Paramecium* cells to $nTiO_2$ in the presence of *E. coli*, and (3) feeding of *Paramecium* cells with $nTiO_2$-preloaded *E. coli*.

The experimental setup included: *Paramecium* alone, *Paramecium* + *E. coli* and $nTiO_2$ without cells (Control; Group 1), *Paramecium* + $nTiO_2$ and *Paramecium* + *E. coli* + $nTiO_2$ (Treatment; Group 2) and *Paramecium* + $nTiO_2$-preloaded *E. coli* (Treatment; Group 3).

The experiments were performed in 6-well plates, and each well contained 3 ml of Dryl's buffer with *Paramecium* (600–800 cells/ml) and/or *E. coli* (OD_{600} 0.4). *Paramecium* in the treatment group was exposed to different concentrations (5, 25, 50 and 100 μg/ml) of $nTiO_2$. The cellular internalisation of $nTiO_2$ was assessed using flow cytometry and validated by both bright field and transmission electron microscopy. Each sample was analysed after 1 h of exposure and subsequently every 2 h until experimental completion (9 h). Additionally, samples from Group 3 were also analysed at 24 h to verify the dilution of NPs in the cells because the dilution was not evaluated at 9 h.

The details regarding sample preparation and flow cytometry data analysis are given in the supplementary information (SI method section 5).

***Paramecium* sample preparation for dark field, bright field and transmission electron microscopy.** Detailed protocols for the sample preparation of *Paramecium* for dark field, bright field and transmission electron microscopy are given in the supplementary information (SI method section 4.1 and 4.3).

Statistical analysis. The three independent experiments were performed for all assays, and the results were expressed as the mean ± standard error (SE). Statistical analysis was carried out using Microsoft Excel 2007 and GraphPad Prism version 3.02. The significance of the data were analysed using one-way analysis of variance (ANOVA) with Dunnett's post hoc test as well as t-tests (non-parametric). In all cases, $p < 0.05$ was considered significant.

References

1. Lazareva, A. & Keller, A. A. Estimating potential life cycle releases of engineered nanomaterials from wastewater treatment plants. *ACS Sustainable Chem. Eng* **2,** 1656–1665 (2014).
2. Vance, M. E. *et al.* Nanotechnology in the real world: Redeveloping the nanomaterial consumer products inventory. *Beilstein J Nanotechnol* **6,** 1769–1780 (2015).
3. Liu, H. H., Bilal, M., Lazareva, A., Keller, A. & Cohen, Y. Simulation tool for assessing the release and environmental distribution of nanomaterials. *Beilstein J Nanotechnol* **6,** 938–51 (2015).
4. Gottschalk, F. & Nowack, B. The release of engineered nanomaterials to the environment. *J Environ Monit* **13,** 1145–55 (2011).
5. Holden, P. A. *et al.* Ecological nanotoxicology: integrating nanomaterial hazard considerations across the subcellular, population, community, and ecosystems levels. *Acc Chem Res* **46,** 813–22 (2013).
6. Weir, A., Westerhoff, P., Fabricius, L., Hristovski, K. & von Goetz, N. Titanium dioxide nanoparticles in food and personal care products. *Environ Sci Technol* **46,** 2242 (2012).
7. Shi, H., Magaye, R., Castranova, V. & Zhao, J. Titanium dioxide nanoparticles: a review of current toxicological data. *Part Fibre Toxicol* **10,** 15 (2013).
8. Lee, J., Mahendra, S. & Alvarez P. J. J. Nanomaterials in the construction industry: A review of their applications and environmental health and safety considerations. *ACS-Nano* **4,** 3580–3590 (2010).
9. Gnanaprakasam, A., Sivakumar, V. M., Sivayogavalli, P. L. & Thirumarimurugan, M. Characterization of TiO_2 and ZnO nanoparticles and their applications in photocatalytic degradation of azodyes. *Ecotoxicol Environ Saf*, doi: 10.1016/j.ecoenv (2015).
10. Morabito, K., Shapley, N. C., Steeley, K. G. & Tripathi, A. Review of sunscreen and the emergence of non-conventional absorbers and their applications in ultraviolet protection. *Int J Cosmet Sci* **33,** 385–90 (2011).

11. Gulson, B., McCall, M. J., Bowman, D. M. & Pinheiro, T. A review of critical factors for assessing the dermal absorption of metal oxide nanoparticles from sunscreens applied to humans, and a research strategy to address current deficiencies. *Arch Toxicol*, doi: 10.1007/s00204-015-1564-z (2015).
12. Maurer-Jones, M. A., Gunsolus, I. L., Murphy, C. J. & Haynes, C. L. Toxicity of engineered nanoparticles in the environment. *Anal Chem* **85,** 3036–49 (2013).
13. Gottschalk, F., Ort, C., Scholz, R. W. & Nowack, B. Engineered nanomaterials in rivers-exposure scenarios for Switzerland at high spatial and temporal resolution. *Environ Pollut* **159,** 3439–45 (2011).
14. Pernthaler, J. Predation on prokaryotes in the water column and its ecological implications. *Nat Rev Microbiol* **3,** 537–46 (2005).
15. Mullen, M. D., Wolf, D. C., Ferris, F. G., Beveridge, T. J., Flemming, C. A. & Bailey, G. W. Bacterial sorption of heavy metals. *Appl Environ Microbiol* **55,** 3143–9 (1989).
16. Batley, G. E., Kirby, J. K. & McLaughlin, M. J. Fate and risks of nanomaterials in aquatic and terrestrial environments. *Acc Chem Res* **46,** 854–62 (2013).
17. Hoet, P. H., Nemmar, A. & Nemery, B. Health impact of nanomaterials? *Nat Biotechnol* **22,** 19 (2004).
18. Werlin, R. *et al.* Biomagnification of cadmium selenide quantum dots in a simple experimental microbial food chain. *Nat Nanotechnol* **6,** 65–71 (2011).
19. Holbrook, R. D., Murphy, K. E., Morrow, J. B. & Cole, K. D. Trophic transfer of nanoparticles in a simplified invertebrate food web. *Nat Nanotechnol* **3,** 352–355 (2008).
20. Zhu, X., Chang, Y. & Chen, Y. Toxicity and bioaccumulation of TiO_2 nanoparticle aggregates in Daphnia magna. *Chemosphere* **78,** 209–215 (2009).
21. Zhu, X., Wang, J., Zhang, X., Chang, Y. & Chen, Y. Trophic transfer of TiO(2) nanoparticles from Daphnia to zebrafish in a simplified freshwater food chain. *Chemosphere* **79,** 928–933 (2010).
22. Wang, Y. *et al.* Bioaccumulation of CdTe quantum dots in a freshwater alga Ochromonas danica: a kinetics study. *Environ Sci Technol* **47,** 10601–10610 (2014).
23. Bouldin, J. L. *et al.* Aqueous toxicity and food chain transfer of Quantum DOTs in freshwater algae and Ceriodaphnia dubia. *Environ Toxicol Chem* **27,** 1958–1963 (2008).
24. Conway, J. R., Hanna, S. K., Lenihan, H. S. & Keller, A. A. Effects and implications of trophic transfer and accumulation of CeO_2 nanoparticles in a marine mussel. *Environ Sci Technol* **48,** 1517–1524 (2014).
25. Manke, A., Wang, L. & Rojanasakul, Y. Mechanisms of nanoparticle-induced oxidative stress and toxicity. *Biomed Res Int* **2013,** 942916 (2013).
26. Zhang, W., Stack, A. G. & Chen, Y. Interaction force measurement between E. coli cells and nanoparticles immobilized surfaces by using AFM. *Colloids Surf B Biointerfaces* **82,** 316–324 (2011).
27. Pagnout, C. *et al.* Role of electrostatic interactions in the toxicity of titanium dioxide nanoparticles toward Escherichia coli. *Colloids Surf B Biointerfaces* **92,** 315–321 (2012).
28. El Badawy, A. M. *et al.* Surface charge-dependent toxicity of silver nanoparticles. *Environ Sci Technol* **45,** 283–287 (2011).
29. Arvizo, R. R. *et al.* Effect of nanoparticle surface charge at the plasma membrane and beyond. *Nano Lett* **10,** 2543–2548 (2010).
30. Holden, P. A., Schimel, J. P. & Godwin, H. A. Five reasons to use bacteria when assessing manufactured nanomaterial environmental hazards and fates. *Curr Opin Biotechnol* **27,** 73–78 (2014).
31. Chojnacka, K. Biosorption and bioaccumulation–the prospects for practical applications. *Environ Int* **36,** 299–307 (2010).
32. Zhang, W., Rittmann, B. & Chen, Y. Size effects on adsorption of hematite nanoparticles on E. coli cells. *Environ Sci Technol* **45,** 2172–8 (2011).
33. Ghafari, P. *et al.* Impact of carbon nanotubes on the ingestion and digestion of bacteria by ciliated protozoa. *Nature Nanotech* **3,** 347–351 (2008).
34. Zhang, W., Hughes, J. & Chen, Y. Impacts of hematite nanoparticle exposure on biomechanical, adhesive, and surface electrical properties of Escherichia coli cells. *Appl Environ Microbiol* **78,** 3905–3915 (2012).
35. Li, K. *et al.* Surface interactions affect the toxicity of engineered metal oxide nanoparticles toward Paramecium. *Chem Res Toxicol* **25,** 1675–1681 (2012).
36. Ma, S., Zhou, K., Yang, K. & Lin, D. Hetero-agglomeration of oxide nanoparticles with algal cells: effects of particle type, ionic strength and pH. *Environ Sci Technol* **49,** 932–9 (2015).
37. Brayner, R. *et al.* Toxicological impact studies based on Escherichia coli bacteria in ultrafine ZnO nanoparticles colloidal medium. *Nano Lett* **6,** 866–870 (2006).
38. Rao, J. V., Srikanth, K., Arepalli, S. K. & Gunda, V. G. Toxic effects of acephate on Paramecium caudatum with special emphasis on morphology, behaviour, and generation time. *Pesticide biochemistry and physiology* **86,** 131–137 (2006).
39. Mudunkotuwa, I. A. & Grassian, V. H. Citric acid adsorption on TiO_2 nanoparticles in aqueous suspensions at acidic and circumneutral pH: surface coverage, surface speciation, and its impact on nanoparticle-nanoparticle interactions. *J. Am. Chem. Soc.* **132,** 14986–14994 (2010).
40. Planchon, M. *et al.* Exopolysaccharides protect Synechocystis against the deleterious effects of titanium dioxide nanoparticles in natural and artificial waters. *J Colloid Interface Sci* **405,** 35–43 (2013).
41. Horst, A. M. *et al.* Dispersion of TiO_2 nanoparticle agglomerates by *Pseudomonas aeruginosa*. *Appl Environ Microbiol* **76,** 7292–7298 (2010).
42. Khan, S. S., Srivatsan, P., Vaishnavi, N. Mukherjee, A. & Chandrasekaran, N. Interaction of silver nanoparticles (SNPs) with bacterial extracellular proteins (ECPs) and its adsorption isotherms and kinetics. *J Hazard Mater* **192,** 299–306 (2011).
43. Jucker, B. A., Zehnder, A. J. & Harms, H. Quantification of polymer interactions in bacterial adhesion. *Envron Sci Technol* **32,** 2909–2915 (1998).
44. Li, B. K. & B. E. Logan. Bacterial adhesion to glass and metal-oxide surfaces. *Colloids Surf. B Biointerfaces* **36,** 81–90 (2004).
45. Hahn, M. W., Lünsdorf, H. & Janke, L. Exopolymer production and microcolony formation by planktonic freshwater bacteria: defence against protistan grazing. *Aquatic microbial ecology* **35,** 297–308 (2004).
46. French, R. A., Jacobson, A. R., Kim, B., Isley, S. L., Penn, R. L. & Baveye, P. C. Influence of ionic strength, pH, and cation valence on aggregation kinetics of titanium dioxide nanoparticles. *Environ Sci Technol* **43,** 1354–9 (2009).
47. Afrooz, A. R., Khan, I. A., Hussain, S. M. & Saleh, N. B. Mechanistic heteroaggregation of gold nanoparticles in a wide range of solution chemistry. *Environ Sci Technol* **47,** 1853–60 (2013).
48. Roberts, A. M. The mechanics of gravitaxis in *Paramecium*. *J Exp Biol* **213,** 4158–4162 (2010).
49. Ford, R. M. & Harvey, R. W. Role of chemotaxis in the transport of bacteria through saturated porous media. *Advances in Water Resources* **30,** 1608–1617 (2007).
50. Labille, J., Harns, C., Bottero, J. Y. & Brant, J. Heteroaggregation of titanium dioxide nanoparticles with natural clay colloids. *Environ Sci Technol* **49,** 6608–16 (2015).
51. Chan, T. S. *et al.* Carbon nanotube compared with carbon black: effects on bacterial survival against grazing by ciliates and antimicrobial treatments. *Nanotoxicology* **7,** 251–8 (2013).
52. Cross, R. K., Tyler, C. & Galloway, T. S. Transformations that affect fate, form and bioavailability of inorganic nanoparticles in aquatic sediments. *Environmental Chemistry* **12,** 627–642 (2015).
53. Hahn, M. W. & Hofle, M. G. Grazing of protozoa and its effect on populations of aquatic bacteria. *FEMS Microbiol Ecol* **35,** 113–121 (2001).

54. del Giorgio, P. A., Gasol, J. M., Vaque, D., Mura, P., Agusti, S. & Duarte, C. M. Bacterioplankton community structure: protists control net production and the proportion of active bacteria in a coastal marine community. *Limnology and Oceanography* **41,** 1169–1179 (1996).
55. Gasol, J. M., Del Giorgio, P. A., Massana, R. & Duarte, C. M. Active versus inactive bacteria: size-dependence in a coastal marine plankton community. *Marine Ecology Progress Series* **128,** 91–97 (1995).
56. Neale, P. A., Jamting, A. K., O'Malley, E., Herrmann, J. & Escher, B. I. Behaviour of titanium dioxide and zinc oxide nanoparticles in the presence of wastewater-derived organic matter and implications for algal toxicity. *Environ Sci: Nano*, doi: 10.1039/C4EN00161C (2014).
57. Kumar, A., Pandey, A. K., Singh, S. S., Shanker, R. & Dhawan, A. A flow cytometric method to assess nanoparticle uptake in bacteria. *Cytometry A* **9,** 707–712 (2011).
58. Shukla, R. K., Sharma, V., Pandey, A. K., Singh, S., Sultana, S. & Dhawan, A. ROS-mediated genotoxicity induced by titanium dioxide nanoparticles in human epidermal cells. *Toxicol In Vitro* **25,** 231–41 (2011).
59. Fok, A. K., Lee, Y. & Allen, R. D. The correlation of digestive vacuole pH and size with the digestive cycle in *Paramecium caudatum*. *The Journal of Protozoology*, **29,** 409–414 (1982).
60. Ali, T. H. & Saleh, D. S. A simplified experimental model for clearance of some pathogenic bacteria using common bacterivorous ciliated spp. in Tigris river. *Applied Water Science* **4,** 63–71 (2014).

Acknowledgements

The authors acknowledge funding from CSIR Network Projects NWP35 and BSC0112 (NanoSHE), India, and the EU-FP7/2007-2013/Grant Agreement 263147 (NanoValid-Development of reference methods for hazard identification, risk assessment and LCA of engineered nanomaterials), Europe. Funding received from the GICT, India, under the CENTRA project Grant Agreement (ILS/GICT/2013/003) is also acknowledged. GSG acknowledges UGC, India, for a Junior Research Fellowship. The CSIR-IITR and DBLS-Ahmedabad University manuscript communication numbers are 3345 and DBLS 65, respectively.

Author Contributions

R.S. conceptualised the experimental design. A.D. discussed the experimental design and critically evaluated the manuscript. G.S.G. executed the experiments. A.K. helped with flow cytometry analysis. All authors contributed to the writing of the manuscript.

Additional Information

Supplementary information accompanies this paper at http://www.nature.com/srep

Competing financial interests: The authors declare no competing financial interests.

How to cite this article: Gupta, G. S. *et al.* Assessment of agglomeration, co-sedimentation and trophic transfer of titanium dioxide nanoparticles in a laboratory-scale predator-prey model system. *Sci. Rep.* **6**, 31422; doi: 10.1038/srep31422 (2016).